Magnetotransport in low-density *p*-Si/SiGe heterostructures: From metal through hopping insulator to Wigner glass

I. L. Drichko,[1,*] A. M. Dyakonov,[1] I. Yu. Smirnov,[1] A. V. Suslov,[2] Y. M. Galperin,[1,3,4] V. Vinokur,[4] M. Myronov,[5] O. A. Mironov,[6] and D. R. Leadley[7]

[1]*A. F. Ioffe Physico-Technical Institute, Russian Academy of Sciences, 194021 St. Petersburg, Russia*

[2]*National High Magnetic Field Laboratory, Tallahassee, Florida 32310, USA*

[3]*Department of Physics and Center for Advanced Materials and Nanotechnology, University of Oslo, P.O. Box 1048 Blindern, 0316 Oslo, Norway*

[4]*Argonne National Laboratory, 9700 S. Cass Avenue, Argonne, Illinois 60439, USA*

[5]*Musashi Institute of Technology, 8-15-1 Todoroki, Setagaya-ku, Tokyo 158-0082, Japan*

[6]*Warwick SEMINANO R&D Centre, University of Warwick Science Park, Coventry CV4 7EZ, United Kingdom*

[7]*Department of Physics, University of Warwick, Coventry CV4 7AL, United Kingdom*

(Received 29 October 2007; revised manuscript received 28 December 2007; published 28 February 2008)

We study dc and ac transport in low-density *p*-Si/SiGe heterostructures at low temperatures and in a broad domain of magnetic fields up to 18 T. Complex ac conductance is determined from simultaneous measurement of velocity and attenuation of a surface acoustic wave propagating in close vicinity of the two-dimensional hole layer. The observed behavior of dc and ac conductances is interpreted as an evolution from metallic conductance at $B=0$ through hopping between localized states in intermediate magnetic fields (close to the plateau of the integer quantum Hall effect corresponding to the Landau-level filling factor $\nu=1$) to formation of the Wigner glass in the extreme quantum limit ($B \gtrsim 14$, $T \lesssim 0.8$ K).

DOI: 10.1103/PhysRevB.77.085327 PACS number(s): 73.23.−b, 73.50.Rb, 73.43.Qt

I. INTRODUCTION

Electron transport through two-dimensional (2D) semiconductor structures is a subject of long continuous attention. The interest is motivated not only by their technological importance—the two-dimensional layers serve as building blocks for devices of modern micro and nanoelectronics—but, most of all, also by appeal of the fundamental questions that arise in the course of their thorough study. Furthermore, these systems offer an excellent opportunity for analyzing an interplay between the electron-electron interaction and disorder, one of the most fundamental problems of current condensed matter physics. External magnetic field adds yet a "new dimension" to wealth of phenomena exhibited by a two-dimensional electron gas.

One of the most interesting magnetotransport phenomenon existing only in 2D systems is the quantum Hall effect (QHE), which manifests itself as a series of broad plateaus in the dependence of the Hall component ρ_{xy} of the conductance tensor on magnetic field or electron density and vanishing of the transverse component ρ_{xx} at the plateaus, see, e.g., Ref. 1 for a review. In choosing notations, we took magnetic field be parallel to the **z** axis, while the electric field is parallel to the **x** axis.

The orbital energy spectrum of a perfect 2D electron system in a perpendicular magnetic field consists of discrete degenerate Landau levels (LLs), $\varepsilon_n=\hbar\omega_c(n+1/2)$, where $\omega_c=eB/m^*c$ is the cyclotron frequency; B is the external magnetic field, e is the electron charge, m^* is the (cyclotron) effective mass, while c is the light velocity.[2] The degeneracy factor of the levels is just the ratio between the sample area and the effective area $2\pi\hbar c/eB$ occupied by a quantum state. Thus, the filling factor, $\nu=2\pi pc\hbar/eB$, where p is the sheet hole (electron) density, has a meaning of the ratio of the hole (electron) number to the "capacity" of a Landau level. An integer ν means that an integer number of LLs is fully occupied and the chemical potential is located in the gap between them. In the above consideration, we have defined the filling factor *per electron spin*. The external field causes Zeeman splitting, $g^*\mu_B B$, of the levels corresponding to different spins, where μ_B is the Bohr magneton, while g^* is the so-called g factor. If Zeeman splitting exceeds the thermal splitting, k_BT, then the spin-split levels are well resolved. Here, T is the temperature, while k_B is the Boltzmann constant.

The domain where $\nu<1$ and $k_BT \lesssim \hbar\omega_c$ is called the *extreme quantum limit* (EQL). In this domain, the electron states are spin polarized and only the lowest Landau level is partly occupied. The magnetotransport in the EQL region is far from being fully understood. There exist predictions that a 2D system in such situation behaves as a specific "Hall insulator" where the off-diagonal component ρ_{xy} of the resistivity tensor keeps its classical values, while the diagonal component ρ_{xx} diverges at zero temperature.[3] This is in contrast with an ordinary (Anderson or Mott) insulator where both components diverge. Transverse dc conductance of both the Hall and an ordinary insulator at finite temperature is due to the variable-range hopping of electrons (holes) between localized states. It turns out that ac conductivity in this regime is complex, $\sigma^{ac} \equiv \sigma_1 - i\sigma_2$ and $\sigma_2 > \sigma_1 > \sigma_{xx}^{dc} = \rho_{xx}/(\rho_{xx}^2 + \rho_{xy}^2)$.[4] This relation has been experimentally confirmed in GaAs/AlGaAs heterostructures near the conductivity minima in the IQHE regime using probeless acoustic methods to measure ac conductivity.[5] The observed large value of the ratio σ_2/σ_1 was interpreted as a hallmark of hopping conductance since the contribution of extended carriers to σ_2 is extremely small in the studied frequency domain.

The alternative scenario for low-temperature behavior of an interacting 2D system is formation of the Wigner

crystal—periodic distribution of charge carriers.[6] In a pure electron system, an interplay between the kinetic and interaction energies of electrons depends only on their density. At sufficiently low density, the typical interaction energy can exceed the Fermi energy of free electrons, and this is just the domain where the Wigner crystal can be formed. The electron Wigner crystal was observed for the first on the surface of liquid He.[7] It was also identified in Si metal-oxide-semiconductor structures with low electron concentration and high mobility (see Ref. 8) for a review.

An external transverse magnetic field shrinks the electron wave functions and in this way facilitates formation of the Wigner crystal. As a result, in the presence of sufficiently strong magnetic field, two-dimensional electron gas can form the Wigner crystal even at relatively high electron concentration for which at $B=0$, the electron system is a liquid.[9] The Wigner crystallization in magnetic field was studied by many research groups, both experimentally and theoretically. Most of experiments were done using high-quality heterostructures such as n-GaAs/AlGaAs,[10] inversion high-mobility Si films,[8,11] InGaAs/InP heterostructures.[12] The most popular experimental method here is studies of dc I-V curves.

A conventional point of view resulting from the above works was that in realistic 2D systems, the Wigner crystal is strongly distorted by disorder and consists of correlated regions sometimes called "the domains." The whole structure is pinned by disorder forming a glasslike system (see, e.g., Refs. 13 and 14). This *Wigner glass* should exhibit specific nonlinear and hysteretic response to the applied voltage, which is typical for pinned interacting random systems.[15–17] In the presence of ac excitation, electrons vibrate around the pinning centers in a collective fashion forming the so-called *pinning collective mode* strongly influenced by the magnetic field. This mode was identified as a specific resonance in the ac conductance observed in high-mobility n and p-GaAs/AlGaAs heterostructures at $\nu<0.2$, i.e., in the EQL. The typical resonant frequencies were of few gigahertz.[18–21]

The present work is aimed at studies of dc and ac magnetotransports in low-density heterostructures p-Si/SiGe ($p=8\times10^{10}$ cm^{-2}) both in the QHE ($\nu=1$) and EQL regimes. In this material, the ratio between the typical hole-hole interaction energy and the Fermi energy is about 10; an additional advantage is that here the formation of the Wigner crystal is not masked by the liquid phases corresponding to the fractional quantum Hall effect. In addition to conventional dc measurements, we measure velocity and attenuation of a surface acoustic wave (SAW) excited at the surface of a piezoelectric crystal located close to the 2D hole layer in the heterostructure. These measurements conducted at different temperatures and magnetic fields provide a probeless method for studying ac response. This method allows one determining the *complex* ac conductance; it has been previously successfully applied to n-GaAs/AlGaAs for identifying of Wigner crystal.[22] In this way, we will demonstrate the evolution from metallic conductance at $B=0$ through hopping conductance in intermediate magnetic fields to the formation of the Wigner glass in very high magnetic fields.

The paper is organized as follows. In Sec. II, we report the procedures of measurement and data handling. The results are presented in Sec. III and discussed in Sec. IV.

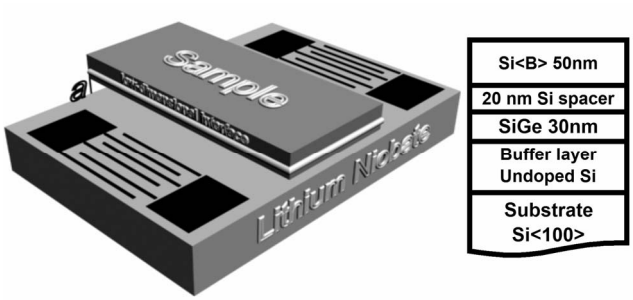

FIG. 1. Sketches of the acoustic experiment setup and sample.

II. EXPERIMENT

A. Procedure

We simultaneously measured attenuation and velocity of SAW in p-Si/SiGe heterostructures with hole density $p=8.2\times10^{10}$ cm^{-2} and mobility $\mu=1\times10^{4}$ cm^2/V s in external magnetic field up to 18 T and temperature interval $T=0.3-4.2$ K. The measurements were performed in the frequency domain $f=18-255$ MHz using the so-called hybrid method (see, e.g., Ref. 5). According to this method, the SAW was excited by an interdigital transducer at the surface of a piezoelectric crystal, $LiNbO_3$, the heterostructure sample being pressed to the surface, as illustrated on Fig. 1. The SAW generates a moving profile of electric field, which penetrates the 2D interface, causing ac electric current. The current produces Joule heating, as well as feedback forces acting upon the elastic medium in the piezoelectric crystal. These processes result in an additional attenuation $\Delta\Gamma$ of the SAW, as well as variation Δv of its velocity. Both effects depend on the conductance of the two-dimensional hole gas (2DHG) at the 2D interface. Consequently, by simultaneous measurement of $\Delta\Gamma$ and Δv, we extract *complex conductivity*, $\sigma^{ac}(\omega)\equiv\sigma_1(\omega)-i\sigma_2(\omega)$, of the 2D hole system versus magnetic field, temperature, and SAW amplitude. This "sandwich" like method allows us to study nonpiezoelectric systems by acoustic methods.

In addition to acoustic experiments, we measured components ρ_{xx} and ρ_{xy} of static electrical resistance, as well as the static current-voltage (I-V) curves of a similar sample in magnetic field up to 18 T and temperatures $T=0.3-2.1$ K.

The pseudomorphic fully strained heterostructure Si⟨B⟩/Si/SiGe/Si/(001)Si was grown using solid source molecular beam epitaxy with e beam on the substrate Si(100) (Fig. 1). It consisted of the 300 nm Si buffer layer followed by 30 nm $Si_{0.92}Ge_{0.08}$ layer, 20 nm undoped spacer, and 50 nm layer of B-doped Si with doping concentration of 2.5×10^{18} cm^{-3}. The 2D interface was located in the strained $Si_{0.92}Ge_{0.08}$ layer (see Ref. 23 for detailed description of the sample).

The samples used for acoustic measurements were of the size 0.3×0.5 cm^2. The dc measurements were performed using a satellite sample made from adjacent sector of the same heterostructure plate and shaped as a Hall bar. Sputtered Al strips annealed at 500 °C for 30 min served as Ohmic potential contacts (see Ref. 24).

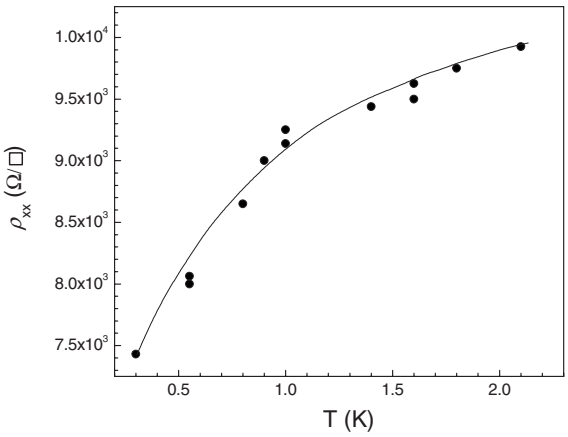

FIG. 2. Temperature dependence of static resistivity ρ_{xx}, $B=0$, and $I=10$ nA. The line is a guide to the eye.

1. Linear regime

a. dc conductivity. Shown in Fig. 2 is the temperature dependence of the static resistivity ρ_{xx} measured at $B=0$ and small measurement current (10 nA). This dependence corresponds to a metal-like behavior, the resistivity at the lowest temperature (0.3 K) being (7.5 ± 0.1) k$\Omega/\square \approx 0.29h/e^2$. In this regime, the I-V curve remains Ohmic up to the current of 300 nA. Thus, one concludes that at $B=0$, the hole system is in a metallic state even at the lowest studied temperature.

The components ρ_{xx} and ρ_{xy} were measured in the temperature domain of 0.3–2 K and in magnetic fields up to 18 T (ρ_{xx}) and 8 T (ρ_{xy}). We were not able to measure ρ_{xy} in larger magnetic fields because there the ρ_{xx} turns out to be too large—1.4 GΩ at $T=0.3$ K and measurement current $I=0.5$ nA. At such resistance, the Hall voltage is masked by potential difference between the voltage probes along the **x** axis.

The components of magnetoresistance versus magnetic field for $B\leqslant 6$ T are shown in Fig. 3. One can notice a minimum in $\rho_{xx}(B)$ at the filling factor $\nu=1$, as well as integer quantum Hall plateaus in ρ_{xy}. There is also a weak dip at $\nu=3$, which is not clearly seen in Fig. 3 because of the chosen scale. The absence of the minima for even values of the filling factor is usual for strained p-SiGe (see, e.g., Ref. 25 and references therein). The reason is the following. While the valence band in p-SiGe is sixfold degenerate if both spin-orbit interaction and strain in the quantum-well structure are neglected, the spin-orbit interaction plus strain partly lift the degeneracy leading to the energy separation of 23 meV between the heavy and light holes.[25] Therefore, the conductivity is maintained by the heavy holes. The spin splitting of the heavy holes in p-SiGe 2D systems is significantly enhanced by exchange interaction. As a result, the spin splitting turns out to be close to the half of the cyclotron splitting, $g^*\mu_B B \approx \hbar\omega_c/2$, where $\omega_c=eB/m^*c$ is the cyclotron frequency. This is why all even dips are suppressed. This behavior strongly differs from that observed in the $A^{III}B^{V}$ heterostructures.

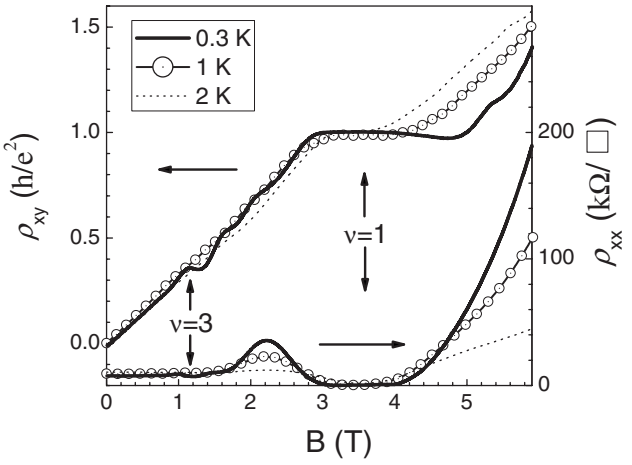

FIG. 3. Magnetic field dependences of ρ_{xx} and ρ_{xy} at different temperatures.

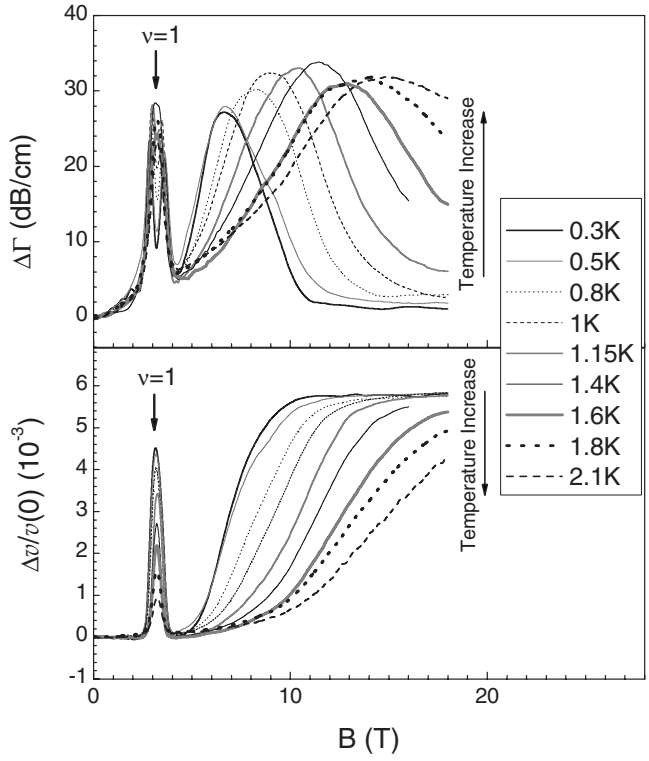

FIG. 4. Magnetic field dependences of $\Delta\Gamma$ and $\Delta v/v(0)$ for different temperatures. $f=87.7$ MHz and $p=8.2\times10^{10}$ cm^{-2}.

At $B\geqslant 4.5$ T and $T\lesssim 10$ K, the holes occupy the states only of lowest spin-split band of the lowest Landau level, so the condition of the quantum limit is fulfilled.

b. Acoustic properties. Shown in Fig. 4 are magnetic field dependences of the acoustic attenuation, $\Delta\Gamma(B)\equiv\Gamma(B)-\Gamma(0)$, and velocity, $\Delta v(B)/v(0)\equiv[v(B)-v(0)]/v(0)$ at $f=87.7$ MHz. Here, $\Gamma(0)$ and $v(0)$ are the SAW attenuation and velocity at $B=0$, respectively. One can see pronounced extremes in both $\Delta\Gamma$ and $\Delta v/v(0)$ at the magnetic field corresponding to $\nu=1$. These extremes coincide with the pronounced dip in static ρ_{xx}, Fig. 3.[26] Above $B\geqslant 4.5$ T, the system is in the extreme quantum limit, $g^*\mu_B B\gtrsim T$. In this region, the attenuation maximum is shifted to larger magnetic fields as temperature increases. This behavior is com-

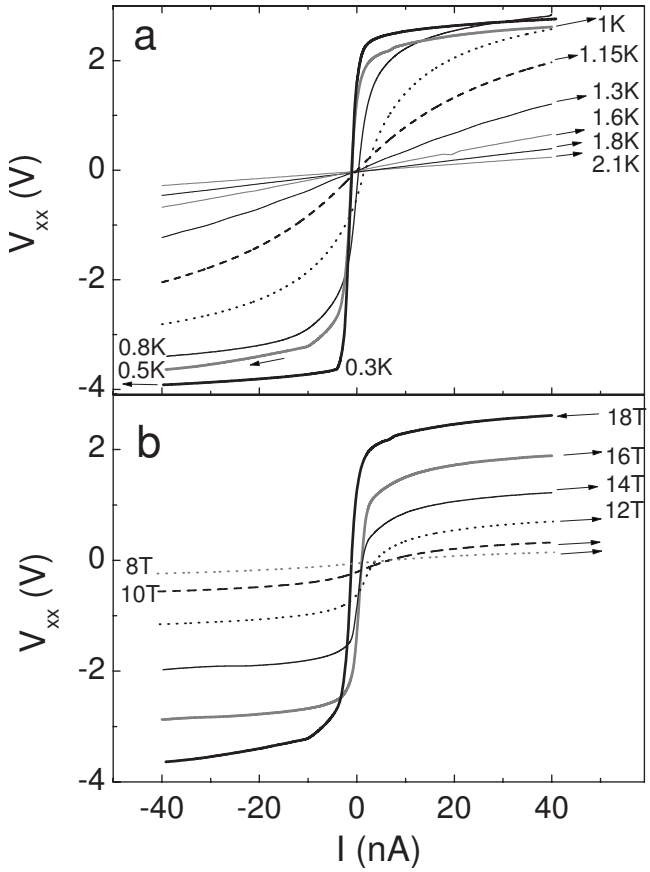

FIG. 5. (a) Voltage-current curves for $B=18$ T and different temperatures. (b) Voltage-current curves for $T=0.55$ K and different magnetic fields. The ramping speed is 5 nA/min. Arrows show the ramping direction.

patible with Eq. (1). Indeed, since the maxima of attenuation are approximately the same for different temperatures, one concludes that $\Sigma_2 \ll 1$. At the same time, $\Sigma_1(B,T)$ being initially large decreases both with magnetic field and temperature (see also Fig. 11). Thus, the larger temperature is the larger magnetic field is needed to fulfill the condition $\Sigma_1 \approx 1$ of the maximal attenuation. The evolution of the attenuation maxima with the acoustic intensity (Fig. 7) can be explained in a similar way. The curves measured at different frequencies (18, 30, 157, and 240 MHz) are similar.

2. Nonlinear regime

a. Voltage-current curves. Shown in Fig. 5 are *V-I* curves for different temperatures and magnetic fields. One can see that the non-Ohmic behavior starts at very low current, the *V-I* curves being asymmetric with respect to the *V* axis showing hysteresis at small currents (see Fig. 6). The sample resistance in the hysteretic region depends on the ramping rate. Note that the voltage-current curves show hysteretic behavior *only* in the domain of magnetic fields and temperatures where they are essentially *nonlinear*.

b. Acoustic properties. The results of acoustic measurements for different SAW intensities are shown in Fig. 7. One can see that in the quantum-limit region, $B \geqslant 4.5$ T, increase in the SAW intensity acts similarly to an increase in temperature. Namely, both the attenuation maximum and saturation of the SAW velocity shift toward large magnetic fields. Similar behaviors are observed at other SAW frequencies.

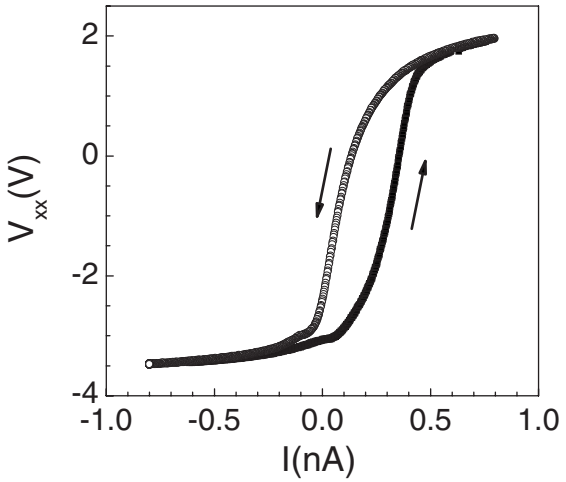

FIG. 6. Hysteretic *V-I* curves measured at $T=0.3$ K and $B=18$ T and ramping speed 0.1 nA/min. Arrows show the ramping direction.

B. Data handling

The components $\sigma_{1,2}$ can be found from simultaneous measurement of $\Delta\Gamma$ and $\Delta v/v(0)$ by solving the set of equations,[5]

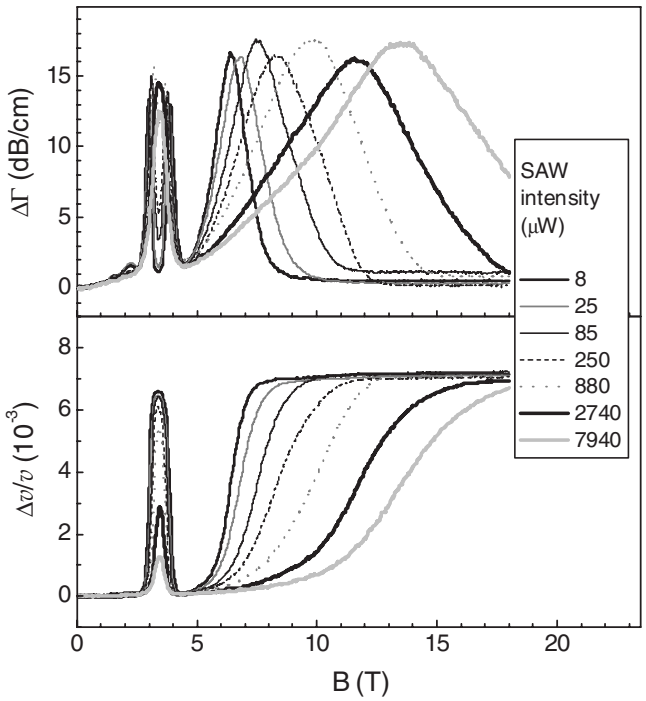

FIG. 7. Magnetic field dependence of $\Delta\Gamma$ and $\Delta v/v(0)$ at different rf-source powers. $T=0.3$ K and $f=30$ MHz.

$$\frac{\Delta\Gamma\ (\mathrm{dB/cm})}{8.68kA(k,a,d)} = \frac{\Sigma_1(B)}{[1+\Sigma_2(B)]^2+\Sigma_1^2(B)} - \frac{\Sigma_1(0)}{[1+\Sigma_1(0)]^2+\Sigma_1^2(0)}, \quad (1)$$

$$\frac{v(B)-v(0)}{v(0)A(k,a,d)} = \frac{1+\Sigma_2(B)}{[1+\Sigma_2(B)]^2+\Sigma_1^2(B)} - \frac{1+\Sigma_2(0)}{[1+\Sigma_1(0)]^2+\Sigma_1^2(0)}, \quad (2)$$

where

$$A(k,a,d) = 110.2b(k,a,d)e^{-2k(a+d)},$$

$$\Sigma_i = 4\pi t(a,k,d)\sigma_i/\varepsilon_s v(0),$$

$$b(k) = \{b_1(k)[b_2(k)-b_3(k)]\}^{-1},$$

$$t(k,a,d) = [b_2(k)-b_3(k)]/2b_1(k),$$

$$b_1(k,a) = (\varepsilon_1+\varepsilon_0)(\varepsilon_s+\varepsilon_0) - (\varepsilon_1-\varepsilon_0)(\varepsilon_s-\varepsilon_0)e^{-2ka},$$

$$b_2(k,d) = (\varepsilon_1+\varepsilon_0)(\varepsilon_s+\varepsilon_0) + (\varepsilon_1+\varepsilon_0)(\varepsilon_s-\varepsilon_0)e^{-2kd},$$

$$b_3(k,a,d) = (\varepsilon_1-\varepsilon_0)(\varepsilon_s-\varepsilon_0)e^{-2ka} + (\varepsilon_1-\varepsilon_0)(\varepsilon_s+\varepsilon_0)e^{-2k(a+d)}, \quad (3)$$

k is the SAW wave vector, d is the depth of the 2D-system layer in the sample, a is the clearance between the sample and the $LiNbO_3$ surface, and $\varepsilon_1=50$, $\varepsilon_0=1$, and $\varepsilon_s=11.7$ are the dielectric constants of $LiNbO_3$, of vacuum, and of the semiconductor, respectively.

The application of Eqs. (1) and (2) is facilitated by the fact that at $B=0$, the conductance is metallic, and in the metallic state, $\sigma_1(\omega)$ is excellently approximated by the static conductance σ^{dc} for all relevant frequencies. Thus, we can calibrate the ac response in the absence of magnetic field by the dc response. For example, for $T=0.3$ K, we set $\sigma_1|_{B=0} = \sigma^{dc}(0) = (1.33\pm0.02)\times10^{-4}\ \Omega^{-1}$. The corresponding value of Σ_1 for the relevant frequency range turns out to be much greater than 1. On the other hand, in the case of metallic conductance, one can expect $\Sigma_2 \ll 1$.[5] Thus, at $B\to0$,

$$\frac{\Delta v(0)}{v(0)A(k,a,d)} \approx \frac{1}{1+\Sigma_1^2} \to 0. \quad (4)$$

At $B\to\infty$, both Σ_1 and Σ_2 vanish and $\Delta v/v(0)$ saturates at the value $A(k,a)$. That is exactly what we see in Fig. 4. Furthermore, we can find $A(k,a)$ from the saturated value of $[\Delta v/v(0)]_{B\to\infty}$. Knowing k, we find from this quantity the clearance a. As an example, at $T=0.3$ K and $f=30$ MHz, the saturated value of $\Delta v/v(0)$ is 7.16×10^{-3} that corresponds to $a=4.3\times10^{-5}$ cm. We have checked that this value agrees with the results for different frequencies—86, 144, 198, and 255 MHz—if the sample was not reinstalled between the measurements. Figure 8 shows the saturation of the SAW velocity $\Delta v/v(0)$ in high magnetic fields at different frequencies. Knowing a, d, and $\sigma^{dc}(0)$, we can calculate $\Gamma(0)$ and, consequently, find the absolute value of the SAW attenuation: $\Gamma(B)=\Delta\Gamma(B)+\Gamma(0)$. This is an important part of the procedure because in high magnetic fields, we cannot find this quantity directly. Indeed, as one can see from Fig. 4, at large magnetic fields, the quantity $\Delta\Gamma$ is very small and the accuracy of its extraction from the raw ac data could be insufficient. Having determined the necessary parameters, we then solve set (1) and (2) for the quantities $\sigma_1(\omega)$ and $\sigma_2(\omega)$.[27]

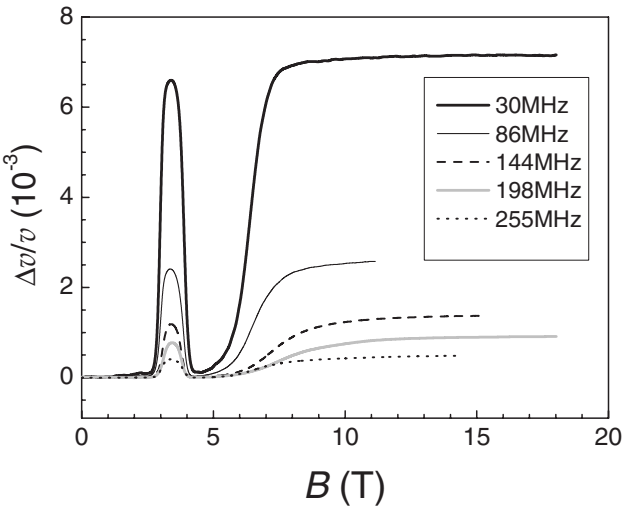

FIG. 8. The SAW velocity shift versus magnetic field at different frequencies at the same sample mounting, $T=0.3$ K.

III. RESULTS

A. Quantum Hall effect regime

Figure 9 illustrates experimental dependences of the real σ_1 and imaginary σ_2 components of the complex ac conductivity derived from the acoustical measurements using Eqs.

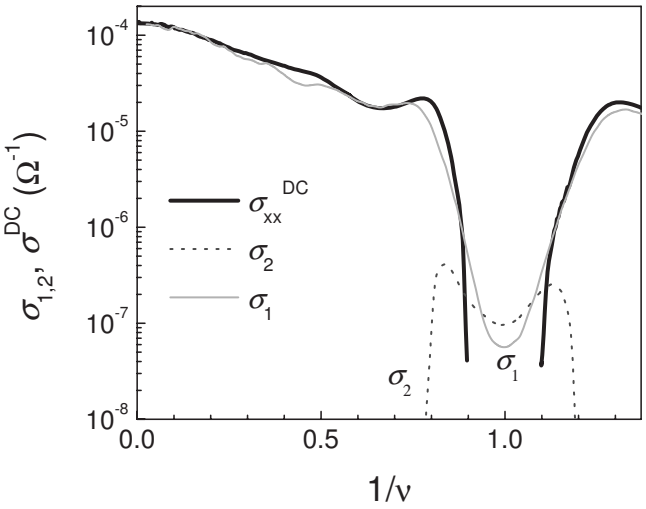

FIG. 9. dc conductivity and real and imaginary components of ac conductivity at 30 MHz on the reversed filling factor in the vicinity of $\nu=1$; $T=0.3$ K.

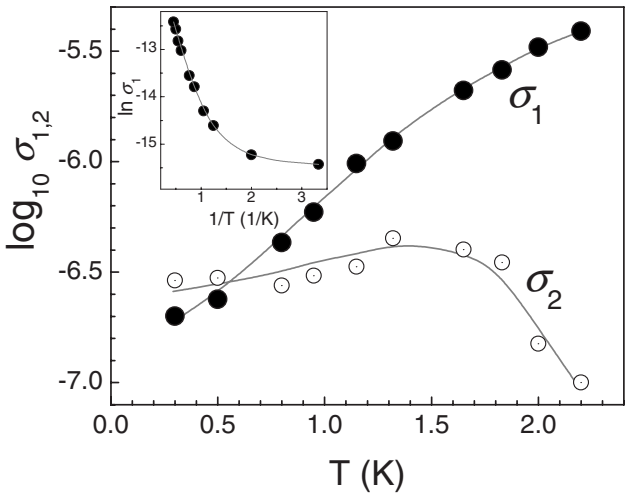

FIG. 10. Real and imaginary components of the ac conductivity versus temperature for $f=18$ MHz and $\nu=1$. Inset: The Arrhenius plot ($\ln \sigma_1$ versus $1/T$) for the same parameters.

(1) and (2), as well as of the dc conductivity, $\sigma_{xx}^{dc}=\rho_{xx}/(\rho_{xx}^2+\rho_{xy}^2)$, on the reciprocal filling factor $1/\nu \propto B$ at $T=0.3$ K in the vicinity of the filling factor $\nu=1$. As follows from this figure, outside the vicinity of $\nu=1$, the values of σ^{dc} and σ_1 are close. This is exactly the region of metallic conductance where the hole states are extended. The situation dramatically changes close to $\nu=1$, where $\sigma_1 \gg \sigma^{dc}$. In addition, in this region the imaginary component σ_2 of the ac conductivity becomes noticeable. Note that at the magnetic field corresponding $\nu=1$, the dimensionless conductivity $\Sigma_1(B) \ll 1$, while outside the close vicinity of $\nu=1$, this quantity is very large. According the Eq. (1), both large and small values of Σ_1 correspond to small attenuation. Consequently, with the change of magnetic field, the acoustic attenuation near $\nu=1$ has two maxima corresponding to two values of B where $\Sigma_1 \approx 1$ and shown in Figs. 4 and 7 as a split peak.

In Fig. 10, the components σ_1 and σ_2 are plotted as functions of temperature for $B=3.2$ T ($\nu=1$) and $f=18$ MHz. One can see that the ratio σ_1/σ_2 increases with temperature. We believe that the low-temperature region where $\sigma_2 > \sigma_1 > \sigma^{dc}$ corresponds to the hopping of the holes between localized states in the random potential produced by charged impurities.[4] We observe that the ac hopping conductance is suppressed as temperature increases. At highest temperatures ($T=0.8-4.2$ K), the temperature dependence of σ_1 is clearly governed by thermal activation, $\sigma_1 \propto e^{-\Delta E/2k_BT}$, with $\Delta E \approx g^* \mu_B B$ (see inset in Fig. 10).

B. Extreme quantum limit

c. Acoustic properties. Shown in Fig. 11 is the dependence of σ_1 at frequency $f=18$ MHz on inverse temperature, $1/T$, in different magnetic fields. We observe that at $T=0.8-2$ K and $B=8-18$ T, the temperature dependence of σ_1 is well described by the Arrhenius law, $\sigma_1 \propto e^{-\Delta E/T}$, with the activation energy ΔE, increasing with magnetic field (see inset). In this domain of temperatures and magnetic fields,

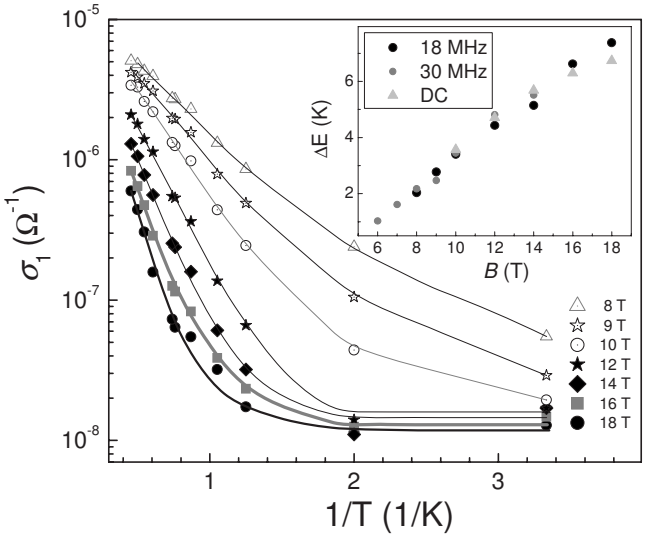

FIG. 11. Dissipative ac conductivity σ_1 versus inverse temperature $1/T$ for different magnetic fields. $f=18$ MHz; the lines are guides for the eye. Inset: magnetic field dependence of the activation energy.

for measured frequencies of 18–157 MHz, $\sigma_1 \approx \sigma^{dc}$ (measured for the current $I=0.5$ nA).

Both quantities depend on temperature according to the Arrhenius law, the activation energies being very close (see Fig. 11, inset). We believe that the observed activation dependences of σ_1 and σ^{dc} are due to magnetic freeze-out of the holes from the extended states of the zeroth Landau level to the states localized nearby the Fermi level. At low temperatures and large magnetic fields ($T<0.8$ K, $B \geqslant 11$ T), the temperature dependence of σ_1 becomes very weak.

Magnetic field dependences of σ_1 at $T=0.3$ K and different frequencies as well as the dc conductivity measured with the current excitation of 0.5 nA are shown in Fig. 12. At $B>8$ T, $\sigma^{dc}/\sigma_1 \ll 1$; this ratio can be less than 0.1. In addition,

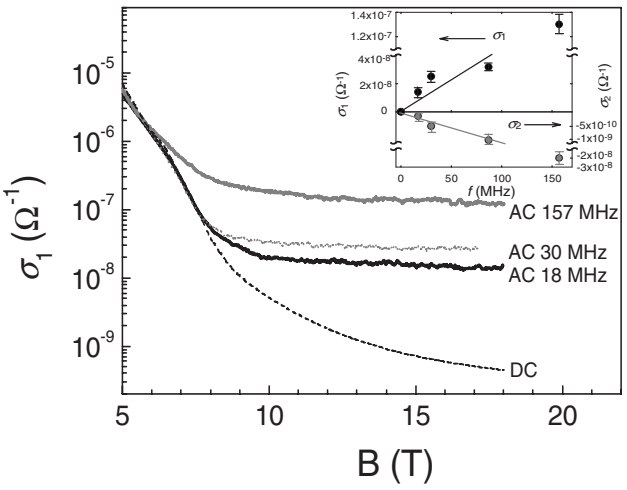

FIG. 12. Real part of the ac conductivity σ_1 at different frequencies and dc conductivity measured at 0.5 nA versus magnetic field; $T=0.3$ K. Inset: frequency dependences of σ_1 and σ_2 at $B=18$ T and $T=0.3$ K.

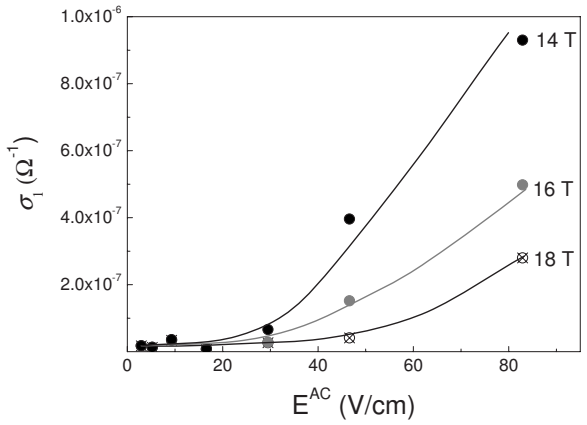

FIG. 13. Dependence of σ_1 on the SAW amplitude E^{ac} at different magnetic fields. $T=0.5$ K and $f=30$ MHz. The lines are guides for the eye.

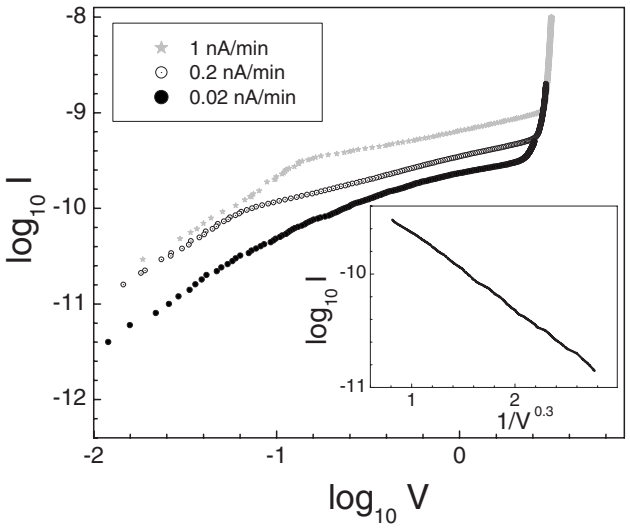

FIG. 14. $\log_{10}-\log_{10}$ plot of the I-V curves with different current sweep rates at $B=18$ and $T=0.3$ K. Inset: Logarithm of the current versus $V^{-0.3}$ for the curve taken on the ramping speed of 0.02 nA/min.

both the temperature and magnetic field dependences of σ^{dc} cannot be accounted for by conventional expressions for hopping conductance. The magnetic field dependence of σ_1 weakens as magnetic field increases; at $B \geqslant 12$ T, the dependence is almost absent.

Inset of Fig. 12 illustrates the frequency dependences of $\sigma_{1,2}$ at $B=18$ T and $T=0.3$ K. The low-frequency parts of these dependences are *linear*: $\sigma_{1,2}(\omega) \propto \omega$. However, the slopes have different signs—the imaginary part of the conductivity σ_2 is *negative*. The experimental points for $f=157$ MHz cannot be allowed for by the linear dependence (note that there is a break in the scale).

Shown in Fig. 13 are dependences of σ_1 on the amplitude E^{ac} of the electric field produced by the SAW in the 2DHG. This amplitude is calculated from the expression[28]

$$(E^{ac})^2 = \frac{32\pi K^2}{v(0)} \frac{W}{l} e^{-2k(a+d)} \frac{kb(k,a,d)(\varepsilon_1+\varepsilon_0)}{(1+\Sigma_2)^2+\Sigma_1^2}. \quad (5)$$

Here, W is the acoustic power carried by the SAW and l is the SAW aperture. The rest of notations is the same as for Eqs. (1) and (2). Though the accuracy of this expression is not high, one can still conclude that in strong magnetic field, the nonlinear behavior starts at higher SAW intensities.

d. dc measurements. Contrary to the case of ac conductance, the non-Ohmic behavior of the static V-I curves (Fig. 5) starts as a threshold. The threshold electric field E_t increases with the magnetic field. At $B=18$ T and $T=0.3$ K, $E_t \approx 9$ V/cm. The threshold positions depend on the ramping speed of the current. However, even at the lowest ramping speed (0.02 nA/min) and smallest currents ($I<0.1$ nA), the V-I curves remain non-Ohmic. Thus, one can conclude that the mechanisms of nonlinear behavior at zero and finite frequency are significantly different.

As we already mentioned, the V-I curves depend on the current ramping rate. To analyze the static nonlinear I-V curves, it is convenient to plot them in the log-log scale. Shown in Fig. 14 is the $\log_{10}$-$\log_{10}$ plot of V-I curves at $B=18$, $T=0.3$ K, and different current sweep rates. The curve with the lowest ramping speed, 0.02 nA/min, can be fitted as

$$I \propto e^{-C/V^{\alpha}}, \quad (6)$$

where C is a constant, while $\alpha=0.3-0.4$ (see inset).

IV. DISCUSSION AND CONCLUSION

From the experimental results and their analysis, we conclude that the conduction mechanisms in p-Si/SiGe heterostructures are different in different domains of temperature and magnetic field.

In the absence of magnetic field, $B=0$, the conductance shows metallic behavior (see Fig. 4). In relatively weak magnetic fields, close to the filling factor $\nu=1$, there is a temperature-driven crossover from the hopping conductance at low temperatures to the thermal activation at higher temperatures. Indeed, at low temperatures ($T<0.6$ K) both $\sigma_1(\omega)$ and $\sigma_2(\omega)$ relatively weakly depend on temperature, and the inequality $\sigma_2 > \sigma_1 > \sigma^{DC}$ holds. This behavior is compatible with the predictions for hopping between the localized states created by the random impurity potential. The results in this domain of the magnetic field and temperature can be allowed for using conventional models for hopping conductance in 2D systems.[4] At $T \gtrsim 1$ K, σ_2 gets much less than σ_1 and finally becomes not measurable, the temperature dependence of σ_1 crosses over to the thermal activation. This behavior is typical for the conductance driven by extended states.

The extreme quantum limit occurs in very strong magnetic fields where $\nu<1$. As follows from Fig. 3, the dc resistance at $B \gtrsim 4.5$ T ($\nu \lesssim 0.8$) increases rapidly with magnetic field. As the temperature increases, the temperature dependence of σ_1 crosses over to thermal activation with magnetic field dependent activation energy (see Fig. 11). This behavior can be understood as a metal-to-insulator transition driven by the magnetic field. A similar transition was

observed by many authors in *p*-Si/SiGe heterostructures (see, e.g., Ref. 25). A crossover from metallic to insulating behavior manifests itself also in the acoustic properties, as seen in Fig. 4—at $B \approx 4.5$ T, both Γ and $\Delta v/v(0)$ cease to depend on temperature. With the increase of temperature, σ_1 crosses over to the Arrhenius law (see Fig. 11). This law holds at $T \gtrsim 1$ K for $B=18$ T and $T \gtrsim 0.5$ K for $B=10$ T.

At the lowest temperature (0.3 K) and 4.5 T $< B <$ 7 T, $\sigma_1 > \sigma_2 > 0$, σ_1 being almost independent of frequency (see Fig. 12). We believe that in this interval of magnetic fields, the process of magnetic freeze-out takes place: Occupation of extended states exponentially decreases with temperature, with the activation energy increasing with magnetic field.

At very high magnetic field and low temperatures, $B > 14$ T and $T < 0.8$ K, we face rather unusual behavior. One could expect that at low temperatures and in very strong magnetic field, the carriers are localized by a random potential; therefore, both dc and ac conductances are due to single-particle hopping between the localized states. This would lead to an exponentially small Ohmic dc conductance σ^{dc}, which should be much less than $\sigma_1(\omega)$. In addition, the predicted σ_2 is positive, and it should significantly exceed σ_1 in the whole studied frequency range.[5] Such a behavior was indeed observed in the vicinity of $\nu=1$, i.e., in the integer quantum Hall effect regime. However, the experimental results for low temperatures and very high magnetic field strongly differ from these predictions. Indeed, the *I-V* curves are nonlinear even for very small voltages. At larger voltages, there is a pronounced increase in the current when the voltage exceeds some threshold value. The *I-V* curves can be described by Eq. (6), which is typical for the creep motion of pinned charge density wave or Wigner glass.[15–17] In the same region of temperatures and magnetic fields, the ac response is linear up to the electric field amplitudes, ~20 V/cm, and we could use the linear theory of acoustic attenuation and velocity change. The linear conductance $\sigma_1 \propto \omega$ is almost independent of temperature and magnetic field. The nonlinear effects are qualitatively similar to those caused by heating of carriers by the electric field created by the SAW. In addition, the imaginary part of the linear-response conductivity is *negative*, and $|\sigma_2| \ll \sigma_1$ that contradicts to the predictions of the model allowing for the single-particle hopping.

We believe that the observed experimental results can be explained assuming that at low temperatures and in strong magnetic field the holes form a *Wigner glass*, i.e., a Wigner crystal distorted by disorder-induced pinning. Indeed, at small voltage and low temperature, the pinned Wigner crystal should behave as an insulator. At finite temperature, parts of the Wigner glass experience correlated hops between different pinned states leading to the charge transfer. This process is similar to the *creep* of dislocations[15] or pinned vortices in type-II superconductors.[16,17] The law [Eq. (6)] and hysteretic *I-V* curves are typical for the creep motion.

The dynamic response of weakly pinned Wigner crystal at not too small frequencies is dominated by the collective excitations[13,14,29] where an inhomogeneously broadened absorption line (the so-called pinning mode) appears.[30] It corresponds to collective vibrations of correlated segments of the Wigner crystal around their equilibrium positions formed by the random pinning potential. The mode is centered at some disorder- and magnetic-field-dependent frequency ω_p, its width being determined by a complicated interplay between different collective excitations in the Wigner crystal. There are modes of two types: transverse (magnetophonons) and longitudinal (magnetoplasmons). The latters include fluctuations in electron density. An important point is that pinning modifies both modes, and the final result depends on the strength and correlation length ξ of the random potential. Depending on the strength and correlation length of the random potential, the frequency ω_p may either increase or decrease with magnetic field. As follows from experiments in GaAs, $\omega_p \approx 10^{10}$ s^{-1} ($f \approx 1.5$ GHz). Consequently, in our acoustic experiments $\omega/\omega_p \ll 1$. Hence, we were not able to observe the peak in the frequency dependence of the attenuation and can discuss only its low-frequency tail. The ratio ω_p/ω_c can be arbitrary. Depending on the interplay between the ratio ω_p/ω_c and the ratio $\eta \equiv \sqrt{\lambda/\beta}$ of the shear (β) and bulk (λ) elastic moduli one can specify two regimes where the behaviors of σ^{ac} are different,

$$1 \ll \omega_c/\omega_{p0} \ll \eta, \tag{7a}$$

$$1 \ll \eta \ll \omega_c/\omega_{p0}. \tag{7b}$$

Here, ω_{p0} is the pinning frequency at $B=0$. As a result, the variety of different behaviors is very rich. Assuming $\xi \gg l_B = (\hbar c/eB)^{1/2}$, one can cast the expression for $\sigma_{xx}(\omega)$ from Ref. 29 into the form

$$\sigma_{xx}(\omega) = i\frac{e^2 n\omega}{m^* \omega_{p0}^2} \frac{1+iu(\omega)}{[1+iu(\omega)]^2 - (\omega\omega_c/\omega_{p0}^2)^2}, \tag{8}$$

where the function $u(\omega)$ is different for regimes (7a) and (7b). Note that the above equation differs from that of Ref. 29 by replacement $\omega \to -\omega$, $u \to -u$ since the sign of ω used in the Fourier transform in Ref. 29 is opposite to that used in Eq. (2).

Below, we will focus on regime (b) since only this regime seems to be compatible with the experimental results. Then,

$$u(\omega) \sim \begin{cases} (\omega/\Omega)^{2s}, & \omega \ll \Omega \quad (9a) \\ \text{const}, & \Omega \ll \omega \ll \omega_c. \quad (9b) \end{cases}$$

Here, $\Omega \sim \omega_{p0}^2 \eta/\omega_c$, while s is some critical exponent. According to Ref. 29, $s=3/2$. For regime Eq. (9b), we have

$$\frac{\sigma_{xx}(\omega)}{\sigma_0} = \frac{\omega}{\omega_{p0}} \frac{i(1+iu)}{(1+iu)^2 - (\eta\omega/\Omega)^2}, \tag{10}$$

where $\sigma_0 \equiv e^2 p/m^* \omega_{p0}$. The result can be cast in the form

$$\sigma_1 = \sigma_0 u \frac{\omega}{\omega_{p0}} \frac{1+u^2+(\eta\omega/\Omega)^2}{[1+u^2+(\eta\omega/\Omega)^2]^2 - (2\eta\omega/\Omega)^2}, \tag{11}$$

$$\sigma_2 = -\sigma_0 \frac{\omega}{\omega_{p0}} \frac{1+u^2-(\eta\omega/\Omega)^2}{[1+u^2+(\eta\omega/\Omega)^2]^2 - (2\eta\omega/\Omega)^2}. \tag{12}$$

The above prediction is qualitatively compatible with the experimental results if one assumes

$$u \gg \omega\omega_c/\omega_{p0}^2 \gg 1. \tag{13}$$

Then,

$$\sigma_1 \approx \sigma_0 \frac{\omega}{u}, \quad \sigma_2 = -\sigma_0 \frac{\omega}{u^2}, \tag{14}$$

and $\sigma_1/|\sigma_2| = u \gg 1$. As follows from the experimental data (see inset of Fig. 12), the components $\sigma_2 < 0$, both σ_1 and σ_2 almost proportional to frequency, and their ratio is $\sigma_1/|\sigma_2| \approx 40$, i.e., greater than 1. In addition, the experimentally measured σ_1 and σ_2 are almost independent of magnetic field and temperature in the domain where we expect the formation of the Wigner crystal.

Regime (14) requires inequalities (13) and (9b) to be met simultaneously. These conditions impose restriction on the frequency ω_{p0} of the collective mode. Indeed, they are both valid if $\omega_{p0} \approx (1.2–1.5) \times 10^{10}$ s^{-1}. In this way one can determine the pinning frequency in the absence of magnetic field. At $\sigma_1/|\sigma_2| \approx 40$ and $B > 14$ T, inequality (13) is valid only for frequencies of 18–90 MHz. At frequency $f = 157$ MHz, the ratio $\omega\omega_c/\omega_{p0}^2$ is much greater than 40. That can explain why the linear frequency dependence of σ_1 and σ_2 does not hold up to the highest experimental frequency. Taking into account low accuracy in determination of σ_2, the agreement between theory and experiment can be considered as satisfactory.

Assuming that $\omega_{p0} = 1.5 \times 10^{10}$ s^{-1}, $u = 40$, and using Eq. (8), one can estimate the concentration of the holes participating in formation of the Wigner crystal in the extreme quantum limit. The estimate yields a value, which is approximately by 2 orders of magnitude smaller, than the hole density in the absence of magnetic field (8.2×10^{10} cm^{-2}). Apparently, in the very strong magnetic field most of carriers is captured by impurities and only small part is involved in formation of the Wigner glass. Unfortunately, we cannot compare this result with any data on Hall resistance ρ_{xy} since we were not able to measure this quantity in the extreme quantum limit.

Knowing the frequency ω_{p0}, we can estimate the typical correlation length L of a pinned Wigner crystal. Following Ref. 31, we have

$$\omega_{p0} = c_t(2\pi/L), \tag{15}$$

where $c_t = \sqrt{\beta/pm^*}$ is the velocity of transverse phonons in the Wigner crystal, m^* is the hole effective mass, and $\beta = 0.245e^2p^{3/2}/\varepsilon_s$ is the shear elastic modulus.

Assuming the effective hole density at $T = 0.3$ K and $B = 18$ T to be $p \approx 10^9$ cm^{-2} (i.e., two orders lower then 2DHG sheet density), one estimates the correlation length as $L \approx 4 \times 10^{-4}$ cm. The lattice constant of the Wigner crystal $a_W \equiv (\pi p)^{-1/2} \approx 4 \times 10^{-5}$ cm. Furthermore, with such p the ratio of the hole-hole interaction energy to the Fermi energy $\kappa = E_{hh}/E_F \approx 70$. Thus, the inequalities which are necessary conditions for the Wigner crystal formation—$L \gg a_W$ and $\kappa \gg 1$—are met.

Though the above estimates produce reasonable numbers one should not overestimate their accuracy. The point is that, along with the "pinning" modes, there exist localized "soft" ones. They appear in the places where pinning is weak.[13,14,29] One can expect that these modes can also contribute to the ac conductance similarly as it happens in structural glasses.[32] Moreover, the frequency dependence of their contribution to $\sigma_1(\omega)$ is close to linear, while the contribution to σ_2 is small. Unfortunately, the density of these soft modes is unknown; therefore, we are not able to estimate these contributions quantitatively.

To conclude the discussion, we believe that p-Si/SiGe heterostructures demonstrate crossover between different mechanisms of dc and ac conductances—from metallic conductance at $B = 0$ through hopping in the integer quantum Hall effect regime to the pinned Wigner crystal (Wigner glass) in the extreme quantum limit (at $B > 14$ T and $T < 0.8$ K). The conclusion regarding formation of the Wigner glass is supported by the behavior of complex ac conductance showing small negative imaginary part compatible with the predictions of Ref. 29 for the pinning mode of a Wigner crystal, as well as by a creeplike nonlinear behavior and hysteretis of dc conductance. This conclusion agrees with that of Ref. 8 based on dc measurements.

ACKNOWLEDGMENTS

We are grateful to V. M. Pudalov and V. I. Kozub for useful discussions and to E. Palm and T. Murphy for their help with the experiments performed at the NHMFL. The work is supported by grants of the Presidium of the Russian Academy of Science, the Program of Branch of Physical Sciences "Spintronika," St. Petersburg Scientific Center of RAS 2007; NSF Cooperative Agreement No. DMR-0084173, State of Florida; and NHMFL In-House Research Program. The work of Y.G. and V.V. was supported by the U.S. Department of Energy Office of Science through Contract No. DE-AC02-06CH11357 and by Norwegian Research Council through USA-Norway bilateral agreement.

*irina.l.drichko@mail.ioffe.ru

[1] *The Quantum Hall Effect*, edited by R. E. Prange and S. M. Girvin (Springer-Verlag, Berlin, 1987).

[2] L. D. Landau and E. M. Lifshits, *Kvantovaya Mechanika* (Fizmatgiz, Moscow, 1963) Vol. 3, p. 704.

[3] O. Viehweger and K. B. Efetov, J. Phys.: Condens. Matter **2**, 7049 (1990); S. Kivelson, D.-H. Lee, and S.-C. Zhang, Phys. Rev. B **46**, 2223 (1992).

[4] A. L. Efros, Zh. Eksp. Teor. Fiz. **89**, 1834 (1985) [JETP **89**, 1057 (1985)].

[5] I. L. Drichko, A. M. Diakonov, I. Yu. Smirnov, Y. M. Galperin, and A. I. Toropov, Phys. Rev. B **62**, 7470 (2000).

[6] E. Wigner, Phys. Rev. **46**, 1002 (1934).

[7] C. C. Grimes and G. Adams, Phys. Rev. Lett. **42**, 795 (1979).

[8] V. M. Pudalov, *Physics of Quantum Electrons Solid* (International, Cambridge, MA, 1994), p. 124.
[9] Y. E. Lozovik and V. I. Yudson, JETP Lett. **22**, 11 (1975) [Pis'ma Zh. Eksp. Teor. Fiz. **22**, 26 (1975)].
[10] H. W. Jiang, H. L. Stormer, D. C. Tsui, L. N. Pfeiffer, and K. W. West, Phys. Rev. B **44**, 8107 (1991).
[11] V. T. Dolgopolov, G. V. Kravchenko, A. A. Shashkin, and S. V. Kravchenko, Phys. Rev. B **46**, 13303 (1992).
[12] B. Pödör, Gy. Kovács, G. Reményi, I. G. Savel'ev, and S. V. Novikov, Inorg. Mater. **37**, 439 (2001).
[13] H. A. Fertig, Phys. Rev. B **59**, 2120 (1999).
[14] M. M. Fogler, Physica E (Amsterdam) **22**, 98 (2004).
[15] L. B. Ioffe and V. M. Vinokur, J. Phys. C **20**, 6149 (1987).
[16] M. V. Feigel'man, V. B. Geshkenbein, A. I. Larkin, and V. M. Vinokur, Phys. Rev. Lett. **63**, 2303 (1989).
[17] G. Blatter, M. V. Feigel'man, V. B. Geshkenbein, A. I. Larkin, and V. M. Vinokur, Rev. Mod. Phys. **66**, 1125 (1994).
[18] F. I. B. Williams, P. A. Wright, R. G. Clark, E. Y. Andrei, G. Deville, D. C. Glattli, O. Probst, B. Etienne, C. Dorin, C. T. Foxon, and J. J. Harris, Phys. Rev. Lett. **66**, 3285 (1991).
[19] P. D. Ye, L. W. Engel, D. C. Tsui, R. M. Lewis, L. N. Pfeiffer, and K. West, Phys. Rev. Lett. **89**, 176802 (2002).
[20] C. C. Li, J. Yoon, L. W. Engel, D. Shahar, D. C. Tsui, and M. Shayegan, Phys. Rev. B **61**, 10905 (2000); C. C. Li, L. W. Engel, D. Shahar, D. C. Tsui, and M. Shayegan, Phys. Rev. Lett. **79**, 1353 (1997).
[21] P. Yong, G. Chen, G. Sambamdamurthy, Z. H. Wang, R. M. Lewis, L. W. Engel, D. C. Tsui, P. D. Ye, L. N. Pfeiffer, and K. West, Nat. Phys. **2**, 452 (2006).
[22] M. A. Paalanen, R. L. Willett, P. B. Littlewood, R. R. Ruel, K. W. West, L. N. Pfeiffer, and D. J. Bishop, Phys. Rev. B **45**, 11342 (1992).
[23] L. Fedina, O. I. Lebedev, G. Van Tendeloo, J. Van Landuyt, O. A. Mironov, and E. H. C. Parker, Phys. Rev. B **61**, 10336 (2000).
[24] S. Agan, O. A. Mironov, M. Tsaousidou, T. E. Whall, E. H. C. Parker, and P. N. Butcher, Microelectron. Eng. **51-52**, 527 (2000).
[25] P. T. Coleridge, Solid State Commun. **127**, 777 (2003).
[26] Small ($\leqslant 10\%$) difference in the peak positions can be attributed to the fact that the samples for dc and acoustic measurements were cut from the neighbouring area of the heterostructure.
[27] According to Eq. (4), $A(k) \propto b(k)$ and the quantity $b(k)$ is very sensitive to the value of the clearance a. For our sample, $b(k)$ decreases by a factor of 10 as a changes from 0.2 to 4 μm at $f=20$ MHz and from 0.2 to 2 μm at $f=200$ MHz. Consequently, the possibility to fit the data for different frequencies by the same value of a provides good verification of our procedure. Note that the accuracy in determining of the clearance a strongly influences the obtained values of σ_2 while σ_1 is less sensitive to a.
[28] I. L. Drichko, A. M. Diakonov, I. Yu. Smirnov, and A. I. Toropov, Semiconductors **34**, 422 (2000) [Fiz. Tekh. Poluprovodn. (S.-Peterburg) **34**, 436 (2000)].
[29] M. M. Fogler and D. A. Huse, Phys. Rev. B **62**, 7553 (2000).
[30] H. Fukuyama and P. A. Lee, Phys. Rev. B **17**, 535 (1978); **18**, 6245 (1978).
[31] B. G. A. Normand, P. B. Littlewood, and A. J. Millis, Phys. Rev. B **46**, 3920 (1992).
[32] S. Hunklinger and W. Arnold, in *Physical Acoustics*, edited by W. P. Mason and R. N. Thurston (Academic, New York, 1976), Vol. XII, p. 155; S. Hunklinger and A. K. Raychaudhuri, in *Progress in Low Temperature Physics*, edited by D. F. Brewer (Elsevier, Amsterdam, 1986), Vol. IX, p. 267.